Proc. Natl. Acad. Sci. USA
Vol. 91, pp. 574–578, January 1994
Biochemistry

The iron-responsive element-binding protein: Localization of the RNA-binding site to the aconitase active-site cleft

(UV cross-linking/base hydrolysis)

JAMES P. BASILION*, TRACEY A. ROUAULT*, CHRISTINA M. MASSINOPLE*, RICHARD D. KLAUSNER*, AND WILSON H. BURGESS†

*Cell Biology and Metabolism Branch, National Institute of Child Health and Human Development, National Institutes of Health, Bethesda, MD 20892; and †Department of Molecular Biology, Holland Laboratory, American Red Cross, Rockville, MD 20855

Contributed by Richard D. Klausner, September 24, 1993

ABSTRACT **The iron-responsive element-binding protein (IRE-BP) binds to specific stem-loop RNA structures known as iron-responsive elements (IREs) present in a variety of cellular mRNAs (e.g., those encoding ferritin, erythroid 5-aminolevulinate synthase, and transferrin receptor). Expression of these genes is regulated by interaction with the IRE-BP. The IRE-BP is identical in sequence to cytosolic aconitase, and the function of the protein is determined by the presence or absence of an Fe–S cluster. The protein either functions as an active aconitase when the Fe–S cluster is present or as an RNA-binding protein when the protein lacks this cluster. Aconitase activity and IRE-binding activity are mutually exclusive, and interconversion between the two activities is determined by intracellular Fe concentrations. Mapping of the RNA-binding site of the IRE-BP by UV cross-linking studies defines a major contact site between IRE and protein in the active-site region. Modeling based on probable structural similarities between the previously crystallized mitochondrial aconitase and the IRE-BP predicts that these residues would be accessible to the IRE only were there a major change in the predicted conformation of the protein when cells are iron-depleted.**

Regulation of gene expression can be largely attributed to specific interactions of proteins with binding sites found within either genomic DNA or RNA transcripts. Cellular regulation of the level of expression of individual genes often depends on the ability of nucleic acid-binding proteins to modulate binding activity in response to developmental or environmental signals. The molecular system that underlies the regulation of expression of genes involved in cellular iron homeostasis has been the subject of extensive work (for review, see refs. 1 and 2). The levels of ferritin, an iron-sequestration protein, and the transferrin receptor, a protein involved in iron uptake, are regulated according to cellular iron availability. A single RNA stem-loop, the iron-responsive element (IRE), located in the 5′-untranslated region of ferritin mRNAs allows iron-regulated control of translation initiation of these mRNAs. The presence of a cluster of IREs in the 3′-untranslated region of the transferrin receptor mRNA confers iron-regulated control of the mRNA half-life. An IRE in the 5′-untranslated region of the mRNA encoding erythroid 5-aminolevulinate synthase, the rate-limiting enzyme in heme synthesis, functions to regulate synthesis of the enzyme and consequently to regulate hemoglobin production (3, 4).

The iron-regulated fate of these mRNA molecules requires interaction with the IRE-binding protein (IRE-BP), which can bind IREs depending on the cellular iron status. When cells are deprived of iron, the protein binds to IREs with high affinity and specificity. However, when the cells are iron replete, the IRE-BP does not bind to IREs. The IRE-BP bears a striking sequence similarity to mitochondrial aconitase (5–7), and it has been established that the IRE-BP is identical to cytosolic aconitase (8). Aconitase is an Fe–S cluster-containing enzyme, in which catalytic activity depends on the presence of an associated [4Fe–4S] cluster. Although the IRE-BP functions as the cytosolic aconitase when the $(Fe–S)_4$ cluster is fully assembled, the form that binds RNA appears to be the apoprotein (9, 10). Thus, IRE-BP switches between an enzyme and an IRE-BP, depending upon the cellular iron status (11). Furthermore, these two states are mutually exclusive. With adequate iron, the protein contains a fully assembled cluster, is a fully active aconitase, and does not bind RNA. Conversely, with iron deprivation the protein appears to lack any cluster, has no aconitase activity, and has full RNA-binding activity.

To begin to understand the interaction between the IRE and its binding protein, we have used UV-radiation-induced cross-links to determine which IRE-BP regions closely associate with the bound IRE. The region of the major RNA–protein contact includes amino acid residues known to contribute to the framework of the active site of the mitochondrial enzyme (12, 13). This information indicates that this cleft is, at least in part, involved with IRE recognition and provides an explanation for the role of the Fe–S cluster in inhibiting RNA binding.

MATERIALS AND METHODS

Purification of IRE-BP. Expression and purification of the IRE-BP were accomplished by using a baculovirus expression system. The entire open reading frame of the human IRE-BP with 72 amino acids derived from a murine cDNA and including a C-terminal thrombin-cleavage site and MYC epitope (14, 15) was cloned into pBlueBac 2 and subsequently used to generate recombinant baculovirus (Invitrogen). Hi-5 insect cells were infected with recombinant baculovirus, and IRE-BP was purified by ion-exchange chromatography from lysates of insect cells overexpressing the IRE-BP (J.P.B., T.A.R., C.M.M., R.D.K., M.C. Kennedy & H. Beinert, unpublished work).

Synthesis of IRE. Radiolabeled or unlabeled IRE RNA was synthesized *in vitro* from a T7 transcription system, as described (Promega; ref. 16). Before use in RNA-hydrolysis analysis, the IRE RNA was purified by ion-exchange chromatography. Synthesized IRE was applied to a Mono Q HR column (Pharmacia) equilibrated with 40 mM KCl/25 mM Tris, pH 8.3/1 mM dithiothreitol and eluted from the column by using a linear salt gradient (40–1000 mM KCl). The sequence of the IRE used was as follows: 5′-GGGAGAG-

The publication costs of this article were defrayed in part by page charge payment. This article must therefore be hereby marked "*advertisement*" in accordance with 18 U.S.C. §1734 solely to indicate this fact.

Abbreviations: IRE, iron-responsive element; IRE-BP, IRE-binding protein; PTH, phenylthiohydantoin.

GAUCCUGCUUCAACAGUGCUUGGACGGAUCC-3'. During synthesis of the IRE, up to four additional 3'-terminal nucleotides were added indiscriminately by the polymerase.

UV Cross-Linking of the RNA–Protein Complex. Fractions containing purified IRE-BP were combined ([protein] = 1.6 mg/ml) and incubated on ice with 1.25 mg of IRE (specific activity, ≈65,000 dpm/μg) for 5–10 min in a final 3.05-ml vol. The mixture was UV-irradiated on ice for 45–60 min in a UV Stratalinker 2400 (Stratagene) at a 12.5-cm distance from the irradiating source (254-nm wavelength).

Purification of IRE-BP–IRE Complex. UV-irradiated IRE-BP–IRE complexes were applied to a Mono Q HR column equilibrated in 40 mM KCl/25 mM Tris, pH 8.3/1 mM dithiothreitol and eluted from the column with a 160-ml linear salt gradient (40–1000 mM KCl) at a flow rate of 2 ml/min. The fractions containing the radiolabeled IRE–IRE-BP complex were identified by SDS/PAGE and scintillation counting, concentrated using a Centricon-30 filtration device (Amicon), and washed with RNase-free water to dilute salts. The concentrated sample was recovered from the concentrator with SDS-loading buffer and fractionated by SDS/PAGE using an 8% (wt/vol) acrylamide gel. The resolved proteins were transferred to nitrocellulose, and the radiolabeled IRE–IRE-BP cross-linked complex was identified by Ponceau S staining and autoradiography.

Digestion, Purification of Radiolabeled Complex, and Peptide Sequencing. The band corresponding to the IRE–IRE-BP complex was cut from the nitrocellulose and digested *in situ*, as described by Aebersold *et al.* (17) with the endoproteinase Asp N (Boehringer Mannheim); the method was modified in that Asp N was resuspended in digestion buffer and incubated at 37°C for 1 hr before addition of RNA–protein complexes to remove endogenous nonspecific nuclease activity. Peptides generated by the enzymatic cleavage were purified on a 30 × 2.1 mm AX-300 column (Applied Biosystems) by using a model 130 microbore HPLC system (Applied Biosystems). RNA–peptide complexes were eluted with a linear gradient of 0–1.0 M KCl in 50 mM sodium phosphate, pH 7.0, and identified by scintillation counting of samples of eluted fractions. Selected fractions were concentrated, and excess salts were removed by ethanol precipitation of the RNA–peptide complex. Amino acid sequence of the isolated peptide complex was determined by using an Applied Biosystems model 477A protein sequencer with an on-line model 120 phenylthiohydantoin (PTH) analyzer.

Labeling and Base Hydrolysis of IRE Associated with Peptide. *RNA preparation.* Unlabeled IRE RNA was synthesized, as described above. IRE RNA was then either 5'- or 3'-end-labeled. For 5'-end-labeling ≈100 μg of IRE RNA was labeled to a specific activity of 1200 × 10^4 cpm/μg, as described in Maniatis *et al.* (18). For 3'-end-labeling, ≈100 μg of IRE RNA was end-labeled to a specific activity of 275 × 10^4 cpm/μg by the method of Krol and Carbon (19). For each protocol the resulting labeled RNA was purified by preparative electrophoresis on an 8 M urea/8% polyacrylamide gel.

Cross-linking and base hydrolysis of RNA. Each of these end-labeled RNAs (1200 × 10^6 cpm for 5'-end-labeled IRE and 275 × 10^6 cpm for 3'-end-labeled IRE) was incubated on ice with ≈2 mg of purified IRE-BP in a 2.2-ml vol. After a 5- to 10-min incubation on ice, the mixtures were irradiated, and the radiolabeled IRE–IRE-BP cross-linked complex was separated and digested with protease, as described above. Approximately 3000–6000 cpm of this digested complex was treated with base (final concentration, 25 mM sodium phosphate, pH 12.0). One-third vol of loading buffer (9.8 M urea/1.5 mM EDTA/0.05% (wt/vol)/xylene cyanol) was added to the samples, and the resulting hydrolysis products were analyzed by electrophoresis on an 8 M urea/20% polyacrylamide gel. Size was assigned to the individual bands by comparison to the migration of IRE digestion products produced by RNase T1 and U2 (United States Biochemical). Base hydrolysis of IRE–peptide complexes was done at 95°C for 20 min for 3'-end-labeled IRE and 15 min at 56°C for 5'-end-labeled RNA. Base hydrolysis of irradiated non-cross-linked RNA was done on RNA retrieved from the Mono Q column.

Modeling of IRE. Modeling was based on a tRNA acceptor stem and T-pseudouridine-C stem-end-loop: (Protein Data Bank code 1TRA) with the program XTALVIEW (20). The CAGUGC loop was modeled by deleting residue 60 on the 3' side of the T-pseudouridine-C loop and adjusting P–P distances of residues 58, 59, and 61 to ≈7 Å. The bulge uridine and cytidine were inserted into the helix maintaining 5.7-Å P–P distances. The model of an IRE was then drawn to scale alongside a ribbon tracing of the crystal structure of mitochondrial aconitase. This modeling was done and provided by C. David Stout (Department of Molecular Biology, Scripps Research Institute, LaJolla, CA.).

RESULTS

Isolation of IRE–IRE-BP Complexes. The epitope-tagged IRE-BP construct was overexpressed in insect cells with a baculovirus expression system. Purification and characterization of the IRE-BP in this system will be described in detail elsewhere. The protein produced was essentially entirely apoprotein, as determined by chemical and spectroscopic means, and was found to bind IREs with affinity and specificity identical to that of endogenous IRE-BP (J.P.B., T.A.R., C.M.M., R.D.K., M.C. Kennedy & H. Beinert, unpublished work). Purified IRE-BP was incubated with a 2-fold molar excess of internally labeled RNA; the RNA used contained the sequence of the human ferritin H chain IRE (21). The RNA–protein mixture was UV-irradiated, and ≈3% of the complexes became covalently linked. Cross-linked material was repurified using the fast protein liquid chromatography Mono Q column to separate free IRE-BP, RNA–IRE-BP complexes, and free IRE RNA. Free protein eluted at ≈250 mM KCl, followed by RNA–protein complexes at

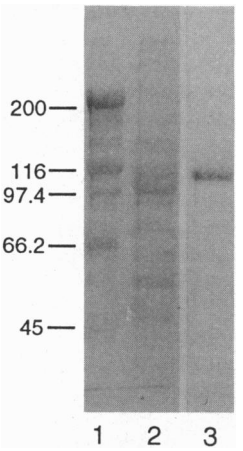

FIG. 1. Separation of cross-linked IRE–IRE-BP complexes from non-cross-linked IRE–IRE-BP complexes. After ion-exchange chromatography, the fractions containing radiolabeled IRE–IRE-BP complexes were concentrated and separated by SDS/PAGE on an 8% (wt/vol) polyacrylamide gel. The resolved complexes were transferred to nitrocellulose, and the IRE–IRE-BP complexes were identified by Ponceau S staining and autoradiography. Lanes: 1, molecular mass standards in kDa; 2, Ponceau S staining of one-tenth of the concentrated fractions containing IRE–IRE-BP complexes; 3, autoradiograph of lane 2. The IRE was internally radiolabeled. The arrowhead indicates migration of cross-linked radiolabeled IRE–IRE-BP complexes. Faster migrating bands probably represent proteolytic breakdown products of the IRE-BP.

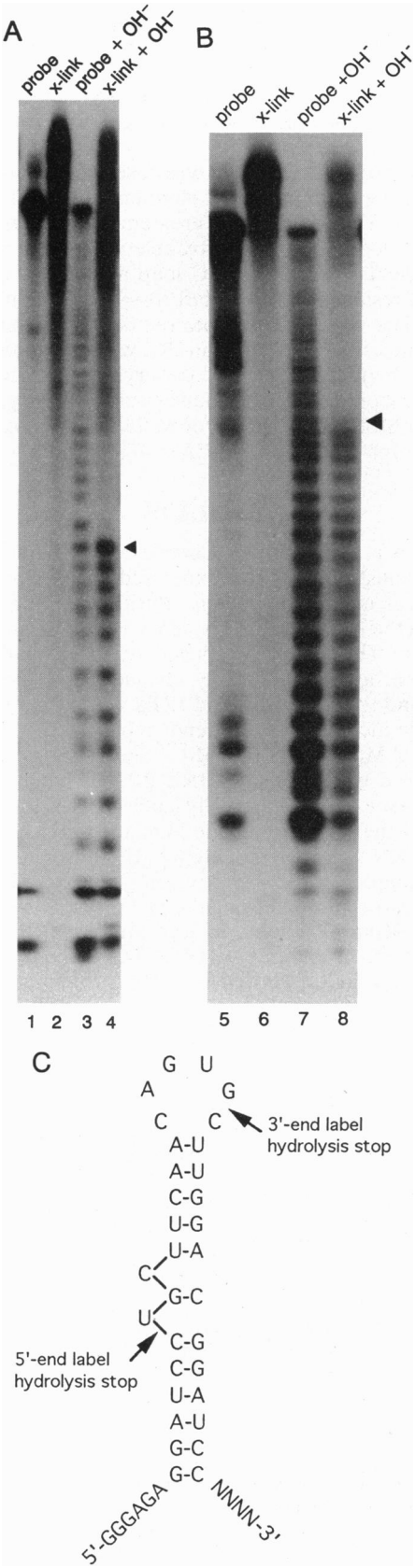

FIG. 2. Base-hydrolysis analysis of IRE RNA cross-linked to peptide DLVIDH-IQV. End-labeled IRE RNA was bound to purified IRE-BP and UV-irradiated; radiolabeled peptide was generated and treated with base, as described. (*A*) Lanes: 1, 5′-^{32}P-IRE without sodium phosphate; 2, 5′-^{32}P-IRE–peptide cross-linked complex without sodium phosphate; 3, alkaline hydrolysis of 5′-^{32}P-IRE; 4, alkaline hydrolysis of 5′-^{32}P-IRE–peptide cross-linked complex. Arrowhead, position in IRE indicated by 5′ arrow in *C*. (*B*) Lanes: 5, 3′-^{32}P-IRE without sodium phosphate; 6, 3′-^{32}P-IRE–peptide cross-linked complex without sodium phosphate; 7, alkaline hydrolysis of 3′-^{32}P-IRE; 8, alkaline hydrolysis of 3′-^{32}P-IRE–peptide cross-linked complex. Arrowhead, position indicated by 3′ arrow in *C*. (*C*) Schematic representation of the ferritin H chain IRE used. Arrows mark the IRE region defined by hydrolysis of the 5′- and 3′-end-labeled IRE–peptide complexes. The 3′-NNNN represents non-template-derived nucleotides added by T7 polymerase during IRE synthesis.

Table 1. Amino acid-sequence analysis of the IRE-containing fraction from the Asp N digest

Cycle	Amino acid	pmol
1	D	4.7
2	L	4.7
3	V	3.2
4	I	4.8
5	D	2.1
6	H	0.7
7	S	ND
8	I	2.5
9	Q	2.7
10	V	0.6

Yields of the PTH-amino acid assigned to each cycle are given. The S in cycle 7 is the expected amino acid in this peptide, although no PTH-serine was detected at this position. ND, none detected.

≈490 mM KCl, and free RNA at ≈660 mM KCl. Purified covalently cross-linked complexes migrated to a position well-separated from unmodified IRE-BP (Fig. 1, lane 2). The radiolabeled RNA was identified by autoradiography and corresponded to the more slowly migrating minor protein species (Fig. 1, lane 3). No detectable protein comigrated with the cross-linked species when protein alone was irradiated (data not shown).

Identification of a Peptide Cross-Linked to the IRE. The region of the nitrocellulose to which the covalent RNA–protein complex was bound was excised and proteolyzed with Asp-N, a protease that cleaves N-terminal to aspartic acids. Peptides spontaneously eluted from the nitrocellulose; 70% of the radioactivity was recovered in the eluate after digestion. The eluate was fractionated by ion-exchange chromatography to exploit the different affinities of the RNA and peptides for the resin. Although most peptides did not bind to the column, the radiolabeled RNA quantitatively bound. The recovered RNA migrated more slowly on a 20% polyacrylamide/8 M urea gel than did radiolabeled RNA processed without IRE-BP, suggesting that the RNA and peptide associated covalently. The radiolabeled fractions were concentrated and sequenced by sequential automated Edman degradation. A single peptide sequence was determined, DLVIDH-IQV, that was identical to the sequence encompassing amino acids 121–130 in human IRE-BP (Table 1), except that no Ser-127 was detected (7, 22). This sequence represents two predicted peptides from the Asp-N digestion with failure to cleave before Asp-125 of the IRE-BP sequence.

Identification of the IRE Region Interacting with Peptide. End-labeled IRE–IRE-BP complex was digested with Asp N, and the cross-linked RNA–peptide complexes were resolved along with free RNA on an 8 M urea/20% polyacrylamide gel. The cross-linked RNA–peptide complex resolved as several distinct species, each migrating more slowly than the free RNA in this gel (Fig. 2, lanes 1, 2 and 5, 6). Base hydrolysis of the samples generated a ladder of RNA-degradation products. Fragment sizes were determined by comparison with RNA oligonucleotides of defined sequence and length generated by digesting IRE RNA with RNases T1 and U2.

Alkaline hydrolysis of the 5′-end-labeled cross-linked complexes (Fig. 2*A*) resulted in an RNA ladder in which all fragments up to 12 nt in length were resolved, but higher-molecular-mass bands precipitously disappeared. Apparent insensitivity to base hydrolysis appeared at position 12 in the sequence of Fig. 2*C*. Base hydrolysis of RNA labeled at the 3′-end, either free or cross-linked to peptide, produced a ladder in which the fragments from the complex matched those from the free RNA until the fragment size was 18 nt (Fig. 2*B*). This result corresponded to position 25 in the IRE sequence in Fig. 2*C*. No effect on base hydrolysis was seen when the irradiated RNA was not cross-linked to protein (Fig. 2, lanes 3 and 7).

DISCUSSION

A major breakthrough that contributed to an understanding of how iron might regulate affinity of the IRE-BP for an IRE came when the IRE-BP was cloned and the protein was found to be very similar to mitochondrial aconitase and identical to the cytosolic form of the enzyme (for review, see refs. 1 and 2). Aconitase is an enzyme, the activity of which depends on a [4Fe–4S] cluster in the active site of the protein (23, 24). Under conditions of high cellular iron, the IRE-BP has an intact [4Fe–4S] cluster, high aconitase activity, and no RNA-binding activity. Conversely, under conditions of low cellular iron the IRE-BP has no Fe–S cluster, no aconitase activity, but has high RNA-binding activity. The goals of our studies were to characterize the RNA-binding site of the IRE-BP and to understand the mechanism by which an intact Fe–S cluster interferes with RNA binding.

To identify specific RNA–protein contacts, we irradiated complexes with UV light, a "zero-length cross-linker" (25, 26), to induce formation of covalent bonds between RNA and protein. The peptide cross-linked to the IRE, DLVIDH-IQV, was identical to amino acids 121–130 in human IRE-BP, except that Ser-127 was not detected. Absence of the PTH-serine may indicate that this amino acid was covalently modified by the cross-linking reactions (27). Other contact points between IRE and IRE-BP may not be identified because some amino acid–nucleotide interactions do not favor formation of covalent bonds during UV irradiation.

Alkaline hydrolysis implicated specific nucleotides in the covalent interaction (Fig. 2*C*). The precipitous change in gel migration of the base-hydrolysis ladder in the area above the arrowhead positions in Fig. 2 *A* and *B* likely results from a mobility shift of the RNA bound to peptide. It is interesting that the RNA region clearly affected by covalently bound peptide contains both the unpaired cytosine of the stem and a region of the loop both of which are conserved and necessary for binding in all functional IREs (1, 28, 29).

Similarities between the IRE-BP and mitochondrial aconitase led us to propose a working model for RNA binding based largely upon the high-resolution crystal structure of mitochondrial aconitase (1, 2). Mitochondrial aconitase is an 83-kDa globular protein consisting of four domains arranged around a central solvent-lined active-site cleft (Fig. 3). The first three N-terminal domains are tightly associated with one another, while the fourth domain is attached to domains one to three via a potentially flexible hinge-linker region. The Fe–S cluster is ligated to three cysteine residues within the third domain, and substrate is bound by amino acids from all four domains (12, 13). The IRE-BP and mitochondrial aconitase are probably structurally quite similar because overall sequence identity is high, active-site residues are conserved, and the specific activities of the enzymes are comparable (7, 8). Amino acid insertions in the IRE-BP relative to mitochondrial aconitase are predicted to lie on the surface in regions of unstructured loops. No insertions interrupt α-helices or β-sheets of the three-dimensional mitochondrial aconitase structure, suggesting that the larger IRE-BP potentially can maintain the core aconitase structure (5).

Inferences concerning the position in the tertiary structure of the DLVIDH-IQV peptide to which the IRE was covalently cross-linked were based on comparing the predicted structure of the IRE-BP to the known structure of the

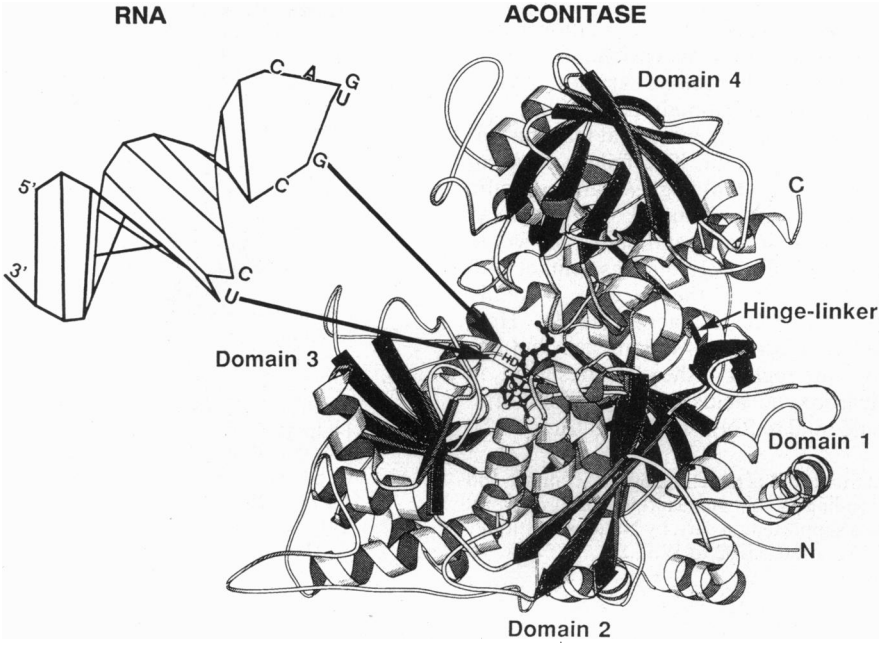

FIG. 3. Scale model of an IRE-like stem-loop and mitochondrial aconitase. An IRE modeled on a stem-loop derived from the crystal structure of tRNA is compared, in scale, to a ribbon trace representation of the crystal structure of mitochondrial aconitase (see text). The hinge-linker that connects domains 1–3 to domain 4 is shown along with the [4Fe–4S] cluster and bound isocitrate. Two arrows indicate the RNA region implicated as interacting with the IRE-BP and converging on the analogous aspartate (D) and histidine (H) amino acids in mitochondrial aconitase found in the peptide generated from IRE–IRE-BP complexes cross-linked by UV irradiation. Only the phosphorous atoms and relevant nucleotides of the RNA are shown.

mitochondrial aconitase. The site of covalent cross-linking on the protein places the RNA deep within the active-site cleft. The amino acids aspartate and histidine (amino acids 125 and 126 in IRE-BP) are active-site residues in aconitase present in the recovered peptide and adjacent to a modified serine (amino acid 127) in the IRE-BP, which may represent the actual site of covalent cross-linking. Other than the two active-site residues, the other residues in this recovered peptide are not present in mitochondrial aconitase, and this region corresponds to an area where an insertion occurs in the sequence relative to mitochondrial aconitase.

To model this interaction, we depict a stem-loop model of an IRE, modeled using a tRNA stem-loop of known dimensions (described in *Materials and Methods*), shown in scale along with a ribbon trace of the 83-kDa mitochondrial aconitase (Fig. 3). Two arrows flank the region of the RNA implicated to interact with the protein by cross-linking studies and point to the analogous region of the active-site cleft of mitochondrial aconitase to which the RNA is bound. In the crystal structure of mitochondrial aconitase, domain 4 is closely apposed to domains 1–3, and the cleft is occupied by direct interactions between amino acid side chains or by ordered solvent molecules. The scale drawing of Fig. 3 indicates that significant conformational changes must occur to accommodate the RNA. Such a model emphasizes the need to "open" the cleft to bind the RNA.

Presence of the Fe–S cluster may antagonize RNA binding in several different ways. The cluster likely imposes local conformational contraints through binding to the three ligating cysteines, one of which (Cys-437) is distant from the other two in the primary sequence. In related work we showed with alkylation studies that Cys-437 is near the RNA-binding site (30). This cysteine is probably located in the tertiary structure of IRE-BP near residues important to RNA binding, and association with the Fe–S cluster may sterically inhibit RNA binding. The intact Fe–S cluster may also antagonize RNA binding by contributing to the binding site of tricarboxylic acid substrates that are bound by residues from all four domains and the cluster. The substrate might, therefore, act as a molecular bridge that favors apposition of domain four to domains one through three. This "closed" conformation would render the RNA-binding site inaccessible.

In summary, when we assume that the tertiary structure of the IRE-BP resembles that of mitochondrial aconitase, the enzymatic active-site cleft appears to provide at least part of the RNA-binding site of this protein. The failure of mitochondrial aconitase to bind IREs (14) suggests that specific contact points in the cleft are not conserved. The proposed model illustrates how an Fe–S cluster and substrate would inhibit RNA binding; binding of the IRE requires contact with residues close to the active site of the enzyme, a totally enclosed region in active mitochondrial aconitase (31). How the RNA is recognized by the protein is still unclear, but it is intriguing that the active-site region of the cleft, designed, in part, to recognize tricarboxylic acids, contains four arginines, residues that could bind to RNA with high affinity (32).

We thank Dr. C. David Stout for his modeling of the aconitase and IRE, for his thoughtful reading of this manuscript, and for helpful suggestions. This work was supported, in part, by National Institutes of Health Grants HL44336 and HL35762 to W.H.B.

1. Klausner, R. D., Rouault, T. A. & Harford, J. B. (1993) *Cell* **72,** 19–28.
2. Klausner, R. D. & Rouault, T. A. (1993) *Mol. Biol. Cell* **4** 1–5.
3. Bhasker, C. R., Burgiel, G., Neupert, B., Emery-Goodman, A., Kuhn, L. C. & May, B. K. (1993) *J. Biol. Chem* **268,** 12699–12705.
4. Melefors, O., Goossen, B., Johansson, H. E., Stripecke, R., Gray, N. K. & Hentze, M. W. (1993) *J. Biol. Chem.* **268,** 5974–5978.
5. Rouault, T. A., Stout, C. D., Kaptain, S., Harford, J. B. & Klausner, R. D. (1991) *Cell* **64,** 881–883.
6. Hentze, M. W. & Argos, P. (1991) *Nucleic Acids Res.* **19,** 1739–1740.
7. Rouault, T. A., Haile, D. H., Downey, W. E., Philpott, C. C., Tang, C., Samaniego, F., Chin, J., Paul, I., Orloff, D., Harford, J. B. & Klausner, R. D. (1992) *BioMetals* **5,** 131–140.
8. Kennedy, M. C., Mende-Mueller, L., Blondin, G. A. & Beinert, H. (1992) *Proc. Natl. Acad. Sci. USA* **89,** 11730–11734.
9. Haile, D. J., Rouault, T. A., Harford, J. B., Kennedy, M. C., Blondin, G. A., Beinert, H. & Klausner, R. D. (1992) *Proc. Natl. Acad. Sci. USA* **89,** 11735–11739.
10. Emery-Goodman, A., Hirling, H., Scarpellino, L., Henderson, B. & Kuhn, L. (1993) *Nucleic Acids Res.* **21,** 1457–1461.
11. Haile, D. J., Rouault, T. A., Tang, C. K., Chin, J., Harford, J. B. & Klausner, R. D. (1992) *Proc. Natl. Acad. Sci. USA* **89,** 7536–7540.
12. Robbins, A. H. & Stout, C. D. (1989) *Proteins* **5,** 289–312.
13. Lauble, H., Kennedy, M. C., Beinert, H. & Stout, C. D. (1992) *Biochemistry* **31,** 2735–2748.
14. Kaptain, S., Downey, W. E., Tang, C., Philpott, C. C., Haile, D. J., Orloff, D. G., Harford, J. B., Rouault, T. A. & Klausner, R. D. (1991) *Proc. Natl. Acad. Sci. USA* **88,** 10109–10113.
15. Rouault, T. A., Tang, C. K., Kaptain, S., Burgess, W. H., Haile, D. J., Samaniego, F., McBride, O. W., Harford, J. B. & Klausner, R. D. (1990) *Proc. Natl. Acad. Sci. USA* **87,** 7958–7962.
16. Milligan, J. F., Groebe, G. W., Witherell, G. W. & Uhlenbeck, O. C. (1987) *Nucleic Acids Res.* **15,** 8783–8798.
17. Aebersold, R. H., Leavitt, J., Saavedra, R. A., Hood, L. E. & Kent, S. B. (1987) *Proc. Natl. Acad. Sci. USA* **84,** 6970–6974.
18. Maniatis, T., Fritsch, E. F. & Sambrook, J. (1989) *Molecular Cloning: A Laboratory Manual* (Cold Spring Harbor Lab. Press, Plainview, NY), pp. 5.68–5.72.
19. Krol, A. & Carbon, P. (1989) *Methods Enzymol.* **180,** 212–227.
20. McRee, D. E. (1992) *J. Mol. Graphics* **10,** 44–47.
21. Hentze, M. W., Caughman, S. W., Rouault, T. A., Barriocanal, J. G., Dancis, A., Harford, J. B. & Klausner, R. D. (1987) *Science* **238,** 1570–1573.
22. Hirling, H., Emery-Goodman, A., Thompson, N., Neupert, B., Seiser, C. & Kuhn, L. C. (1992) *Nucleic Acids Res.* **20,** 33–39.
23. Beinert, H. & Kennedy, M. C. (1989) *Eur. J. Biochem.* **186,** 5–15.
24. Kennedy, M. C., Emptage, M. H., Dreyer, J. L. & Beinert, H. (1983) *J. Biol. Chem.* **258,** 11098–11105.
25. Greenberg, J. R. (1979) *Nucleic Acids Res.* **6,** 715–731.
26. Kinzy, T. G., Freeman, J. P., Johnson, A. E. & Merrick, W. C. (1992) *J. Biol. Chem.* **267,** 1623–1632.
27. Allen, T. D., Wick, K. L. & Matthews, K. S. (1991) *J. Biol. Chem.* **266,** 6113–6119.
28. Leibold, E. A., Laudano, A. & Yu, Y. (1990) *Nucleic Acids Res.* **18,** 1819–1824.
29. Jaffrey, S. R., Haile, D. J., Klausner, R. D. & Harford, J. B. *Nucleic Acids Res.*, in press.
30. Philpott, C. C., Haile, D. J., Rouault, T. A. & Klausner, R. D. (1993) *J. Biol. Chem.* **268,** 17655–17658.
31. Goodsell, D. S., Lauble, H., Stout, C. D. & Olson, A. J. (1993) *Proteins* **17,** 1–10.
32. Tan, R., Chen, L., Buettner, J. A., Hudson, D. & Frankel, A. D. (1993) *Cell* **73,** 1031–1040.